Non-Similar Analysis of Mixed Convection Biomagnetic Boundary Layer Flow Over a Vertical Plate with Magnetization and Localized Heating/Cooling

Rayhan Prodhan[1,5], Mohammad Ferdows[1,*], J. C. Misra[2], Efstratios Tzirtzilakis[3] and M. G. Murtaza[4]

[1]*Research group of Fluid Flow Modeling and Simulation, Department of Applied Mathematics University of Dhaka, Dhaka-1000, Bangladesh*
[2]*Centre for Theoretical Studies, Indian Institute of Technology, Kharagpur-721302, India*
[3]*Fluid Mechanics & Turbomachinery Laboratory, Department of Mechanical Engineering, University of the Peloponnese, Patras, Greece*
[4]*Department of Mathematics, Comilla University, Cumilla 3506, Bangladesh*
[5]*Department of Mathematics, Jashore University of Science and Technology, Jashore-7408, Bangladesh*
E-mail: ferdows@du.ac.bd
[*]*Corresponding Author*

Received 04 May 2023; Accepted 09 February 2024

Abstract

Theoretical and numerical investigation of an applied magnetic field on mixed convection flow of a biofluid through a vertical plate using contained heating or cooling is observed in this study. The mathematical formulation is that of the full Biomagnetic Fluid Dynamics (BFD) model which deals with on the ferrohydrodynamics (FHD) and magnetohydrodynamics (MHD) principle. In this work, the study is performed on a specific biofluid, viz.

European Journal of Computational Mechanics, Vol. 33_2, 91–120.
doi: 10.13052/ejcm2642-2085.3321

human blood. Assume that the magnetization very linearly with magnetic field strength, temperature dependency of dynamic viscosity and thermal conductivity is noticed. A system of non-linear equations with appropriate boundary condition is obtained by familiarizing suitable non-dimensional variables in the physical problem. For the numerical solution, we used finite difference method which is based on an efficient technique is applied in the problem. Computations for flow profiles, local skin friction coefficient and local heat transfer coefficient are performed with the magnetic parameter Mn, the viscosity/temperature parameter θ_r and the thermal/conductivity parameter S^*. The effect of the localized heating or cooling is examined. The computational results presented graphically and have been validated in an appropriate manner. The study reveals that the impact of a magnetic field for blood flow in arteries is found significantly. The results presented bear the promise of valuable applications in physiology, medicine and bioengineering.

Keywords: Magnetization, dipole, convective flow, variability, numerical model.

1 Introduction

Biomagnetic fluid dynamics (BFD) is the investigation of biological fluid under the effect of an applied magnetic field. Numerous research work about the behavior of biomagnetic fluid have been done in health science and bioengineering. Using electromagnetic hyperthermia various investigational medical technique such as heart surgeries, malignancy or tumor treatment, cell separation by developing magnetic field [1–3] and different studies for flow of biomagnetic fluids are of significant interest. Biofluid dynamics may be considered as the discipline of biomedical engineering in which the basic principles of fluid dynamics are used to explain the mechanisms of flows of physiological fluids. The physiological processes take place in human bodies in normal and pathological states.

According to BFD, a strong applied magnetic field affects all biological fluids. A fluid which is found in living organisms that is impacted by the existence of a magnetic field is called a biomagnetic fluid. Blood is the most common biomagnetic fluid found in living humans and subhuman primates, and its flow is influenced by the magnetization of the fluid. Blood is a magnetic fluid due to the presence of iron, proteins, glucose, and cell membrane which is found at a very high concentration in mature red blood cells [4]. Erythrocytes align their disk planes parallel to the magnetic field, according

to experiments [5, 6]. When blood is oxygenated, it behaves as a diamagnetic material, but when it is deoxygenated, it behaves as a paramagnetic substance. Blood has been observed to have magnetic susceptibilities of 3.5×10^{-6} and -6.6×10^{-7} for venous and arterial blood, respectively [7, 8]. Alam et al. [9] observed that magnetic particles are more important in biomedical applications than non-magnetic ones because magnetic particles are readily controlled by magnetic force. The magnetic force makes magnetic particles possible for target molecules attached to reaction mixture particles to be easily and quickly detached from them compared to non-magnetic particles.

The magnetic field's effect on biofluid flow has been extensively studied for bioengineering and medical applications [10, 11], such as controlling blood flow during surgery, cancer treatment, drug targeting, and so on. The study of the hemodynamical flow, considering blood as a homogeneous, Newtonian, electrically non-conducting fluid, was carried out [3, 12]. Haik et al. established the first analytical model for the flow of biomagnetic fluids [13]. Blood was viewed as an electrically non-conducting magnetic fluid in their concept, with flow influenced by fluid magnetization. The model was based on ferrohydrodynamic (FHD) principles, with magnetization assumed to be the dominant force. Magnetohydrodynamics (MHD) principles were used to generate electrically conducting fluids, which, unlike FHD, ignores the polarization and magnetization effect [14]. To account for the magnetic properties of blood, an extended mathematical model for BFD was developed by integrating electrical conductivity and polarization effects. This model can incorporate the energy equation [15, 16] into the study and consider the MHD and FHD properties. Ferdows et al. [17] noticed that, in contrast to MHD and FHD, where ferromagnetic quantities are important over the flow boundary layer, blood temperature was maximum in the case of BFD.

Improved approximation techniques [18] have been proposed for numerical solutions to problems such as the effect of magnetic dipole on the heated ferro-fluid past a stretching sheet [19], the action of localized magnetic field on biomagnetic fluid flow in a rectangular channel [20], and so on. Blood has been reported to exhibit viscoelastic behavior under specific conditions [21–23]. This could be owing to the viscoelastic characteristics of individual erythrocytes and the internal structures produced by cellular connections.

The impact of localized magnetization on bio-magnetic fluid with free/forced convective boundary layer was investigated in [24, 25]. The magnetic field was supposed to be strong enough to consider the bio-magnetic phenomena in this study assuming the magnetization M vary a linearly with magnetic field strength $\vec{H}$. G. M. Murtaza et al. [26] were reported

3-D biomagnetic flow along a stretched sheet in a variable magnetic region and considered M is proportional to temperature T and $\vec{H}$. Merkin and Mahmood [27] analyzed the similarity solution with convection flow over a vertical plate with continuous heat flux. A mathematical model [28] was proposed the impact of magnetic field with mixed convection flow over a vertical plate taking suction/injection into account. Tzirtzilakis et al. [29] observed variable thermal conductivity and viscosity of water-based fluid. Alam et al. [30] investigated the effects of temperature-dependent fluid viscosity and thermal conductivity on blood-Fe_3O_4 flow and heat transfer in the presence of magnetic dipole and found that the blood flow could be regulated by introducing a high magnetic field. The issue of laminar boundary laminar flow and heat transmission in MHD fluids caused by unstable stretched films with prolonged heat flow was examined by Gnaneswara et al. [31]. It is believed that viscosity and thermal conductivity change with temperature. Ashraf et al. [32] examined the physical characteristics of the combined effects of heat generation and absorption from the mobility of nanoparticle material and the influence of different parameters specified by the flow model.

Further investigations of varied problems were carried out by several researchers. The effect of radiation on unstable MHD free convective Flow of Nanofluids across an infinite vertical flat plate was investigated in [33]. The arterial blood flow during physical exercise was studied in [34], blood flow via a small catheterized artery in [35], artery blood flow during electromagnetic hyperthermia [2], effects of MHD on blood flow through a stenosis artery, continuously separates red blood cells from entire blood with a magnetic device [3], medication delivery strategies that target specific parts of the human body, magnetic drug targeting outperforms because of its non-invasive nature and high targeting efficiency [36] are some other similar studies related to flows of biomagnetic fluids.

Andersion and Valnes [37] examined a heated ferrofluid above a stretched sheet in the existence of a magnetic dipole in one of the most classic studies. A BFD flow with non-Newtonian viscoelastic fluid through a stretching sheet in the existence of a magnetic dipole was analyzed by Misra and Shit [38]. Finally, under the influence of an external magnetic field, Misra and Adhikary explored a Bingham plastic fluid with porous media. The application on the pathological view the physical variables were computed in that study in the field of magneto-hemorheology when the system is influence by the exterior magnetic field. Due to the formation of blood clots, in the view of the pathological statement concluded that blood velocity is highest in the plug

(core) area and decreases as blood particles flow near the wall, according to the study [39].

Although as described above, some various researched studies have been carried out in the past, considering various aspects of biomagnetic fluid flow, owing to the prospect of multiple applications of biomagnetic fluid dynamics (BFD), there exist many open problems of this important area of study, which less concern of previous investigators. In view of this, in the present paper we study the viscous flow of a biomagnetic fluid on a vertical plate under the influence of an applied magnetic field with localized heating/cooling. Keeping in view the fact that human body is subject to an applied magnetic field in a variety of situations, e.g. in the case of MRI (Magnetic resonance imaging) and that human blood possesses biomagnetic properties, particular emphasis has been paid to illustrate the applicability of the model developed here by considering blood as the working fluid. Here it may be mentioned that MRI scanners use sufficiently strong magnetic fields and magnetic field gradients [40]. Since the problem is quite complicated, the computational study has been performed by developing a numerical scheme with efficient technique of finite difference method. Results have been presented for the flow and heat transfer profiles, viz. distributions of velocity, temperature, Nusselt number and skin friction. Results corresponding to localized heating/cooling over the vertical plate have been presented.

2 Modeling and Analysis

A mixed convective boundary layer flow in half space $y > 0$ over a heated vertical plate of a steady, viscous incompressible and electrically conducting fluid (biomagnetic) is studied here. We choose the coordinate system $(x - y)$ where x-axis along the plate and y-axis normal to the plate. Consider u_∞ is the free stream fluid velocity and T_∞ is the free stream temperature. Except for a small portion of the plate, the temperature $T_0 (> T_\infty)$ is a constant. The gravitational acceleration g acts in the negative x-direction. The magnetic field is produced by a high-intensity electric current I past a thin electric wire considered along the z-axis and at a distance b below the plate and a far away from the origin. So, the position of the wire is given by

$$(x_0, y_0, z) = (a, b, z) \quad a > 0, b < 0,\ z \in \Re$$

The flow domain is shows in Figure 1.

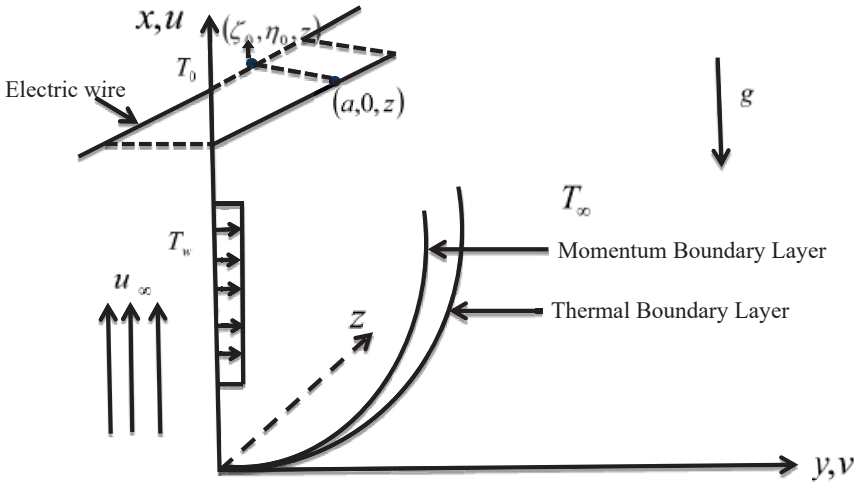

Figure 1 Schematic representation of the model.

The strength of the magnetic field is defined by

$$\|\vec{H}\| = H(x,y) = \frac{I}{2\pi}\frac{1}{[(x-a)^2+(y-b)^2]}.$$

Under the above assumptions, following analogous considerations with [22, 25, 28] the problem equations can be respectively expressed as:

$$\vec{\nabla}\cdot\vec{q} = 0 \tag{1}$$

$$\vec{q}\cdot\vec{\nabla}u = \frac{1}{\rho_\infty}\frac{\partial}{\partial y}\left(\mu\frac{\partial u}{\partial y}\right) + g\beta(T-T_\infty) \pm \frac{\mu_0}{\rho_\infty}M\frac{\partial H}{\partial x} \tag{2}$$

and

$$\vec{q}\cdot\vec{\nabla}T - \frac{\mu_0}{\rho_\infty c_p}T\frac{\partial M}{\partial T}(\vec{q}\cdot\vec{\nabla}H) = \frac{1}{\rho_\infty c_p}\frac{\partial}{\partial y}\left(\kappa\frac{\partial T}{\partial y}\right) \tag{3}$$

The physical problem's boundary conditions can be expressed mathematically in the form

$$\left.\begin{array}{ll} u(x,0)=0, v(x,0)=0, T(x,0)=T_w(x) & \text{for } x_i \le x \le x_j, \\ T(x,0)=T_0 & \text{for } 0 \le x < x_i, x > x_j, \\ u(x,\infty)=u_\infty, & T(x,\infty)=T_\infty, \\ u(0,y)=u_\infty, & T(0,y)=T_\infty, y>0 \end{array}\right\} \tag{4}$$

Where

$$T_w(x) = T_\infty + (T_0 - T_\infty)\left[1 + \frac{\varepsilon(x - x_i)(x_j - x)}{(x_j - x_i)^2}\right] \tag{5}$$

As in [12, 15], consider

$$M = \chi H \tag{6}$$

where χ is the magnetic susceptibility. The fluid exhibits paramagnetic or diamagnetic behavior by taking positive or negative values of χ respectively.

The term in Equation (3), $\frac{\mu_0}{\rho_\infty c_p} T \frac{\partial M}{\partial T}(\vec{q} \cdot \vec{\nabla} H)$ generated by magneto-caloric effect. The last term in Equation (2), viz. $\pm\frac{\mu_0}{\rho_\infty} M \frac{\partial H}{\partial x} = \pm\frac{\mu_0}{\rho_\infty}\chi H \frac{\partial H}{\partial x}$ representing the component of the magnetic force, per unit volume.

Set,

$$\left.\begin{aligned} &\eta(x,y) = \mathrm{Re}_x^{1/2}\frac{y}{x}, y \geq 0, x > 0 \\ &\psi(x,y) = (\upsilon_\infty \mathrm{Re}_x^{1/2}) t(\zeta,\eta) = (\upsilon_\infty x u_\infty)^{1/2} t(\zeta,\eta) \\ &\zeta(x) = \frac{Gr_x}{\mathrm{Re}_x^2} = cx, c = \frac{g\beta(T_0 - T_\infty)}{u_\infty^2} \\ &T(x,y) - T_\infty = (T_0 - T_\infty)\theta(\zeta,\eta) \end{aligned}\right\} \tag{7}$$

where $\zeta(x,y), \eta(x,y)$ are dimensionless functions of x and y, $\psi(x,y)$ is stream function and $T(x,y)$ is temperature. In the above expressions, the local Grashof number, local Reynolds number and the kinematic viscosity are defined by the expressions

$$Gr_x = \frac{g\beta(T_0 - T_\infty)x^3}{\upsilon_\infty^2}, \mathrm{Re}_x = \frac{x u_\infty}{\upsilon_\infty}, \upsilon_\infty = \frac{\mu_\infty}{\rho_\infty}$$

For a viscous fluid, the viscosity depends on the temperature T inversely which is denoted as follows

$$\mu = \frac{\mu_\infty}{1 + \gamma(T - T_\infty)}$$

This equation can be written as follows

$$\frac{1}{\mu} = \alpha(T - T_r) \tag{8}$$

We can write

$$\theta = \frac{T - T_r}{T_0 - T_\infty} + \theta_r \tag{9}$$

where

$$\theta_r = \frac{T_r - T_\infty}{T_0 - T_\infty} = -\frac{1}{\gamma(T_0 - T_\infty)} = \text{constant} \tag{10}$$

κ is the thermal conductivity which is assumed to be linearly proportional to the temperature. So it can be denoted by

$$\kappa = \kappa_\infty[1 + s(T - T_\infty)]$$

where κ_∞ is the thermal conductivity of the surrounding fluid medium, s is constant. This form can be rewritten in the following way:

$$\kappa = \kappa_\infty(1 + S^*\theta) \tag{11}$$

where $S^* = s(T_0 - T_\infty)$

The momentum and energy equations are reduced to,

$$\begin{aligned} t''' - \frac{1}{2}t\frac{\theta - \theta_r}{\theta_r}t'' - \frac{\theta'}{\theta - \theta_r}\left[1 + \frac{\varepsilon(\zeta - \zeta_i)(\zeta_j - \zeta)}{(\zeta_j - \zeta_i)^2}\right]^{-1} t'' \\ - \zeta\theta\left[1 + \frac{\varepsilon(\zeta - \zeta_i)(\zeta_j - \zeta)}{(\zeta_j - \zeta_i)^2}\right]^{-1} \frac{\theta - \theta_r}{\theta_r} \\ = \zeta\frac{\theta - \theta_r}{\theta_r}\left(t''\frac{\partial t}{\partial \zeta} - t'\frac{\partial t'}{\partial \zeta}\right) \\ \mp RMn\frac{(\zeta - ac)\zeta}{[(d\sqrt{\zeta}\eta - cb)^2 + (\zeta - ac)^2]}\frac{\theta - \theta_r}{\theta_r} \end{aligned} \tag{12}$$

$$\frac{1}{\text{Pr}}(1 + S^*\theta)\theta'' + \left(\frac{1}{\text{Pr}}S^*\theta' + \frac{1}{2}t\right)\theta' + \zeta\frac{\partial t}{\partial \zeta}\theta' = \zeta t'\frac{\partial \theta}{\partial \zeta} \tag{13}$$

By using the dimensionless variables (7), the boundary conditions (4) together with (5) are transformed to

$$\left.\begin{array}{ll} t(\zeta,0) = 0, t'(\zeta,0) = 0, \theta(\zeta,0) = 1 + \frac{\varepsilon(\zeta-\zeta_i)(\zeta_j-\zeta)}{(\zeta_j-\zeta_i)^2} & \text{for } \zeta_i \le \zeta \le \zeta_j \\ \theta(\zeta,0) = 1 & \text{for } \zeta < \zeta_i, \zeta > \zeta_j \\ t'(\zeta,\infty) = 1, & \theta(\zeta,\infty) = 0 \end{array}\right\} \tag{14}$$

where, Prandtl number, $\text{Pr} = \frac{\mu_\infty c_p}{\kappa_\infty}$, partially differentiated variable η are denoted by primes., $d = \sqrt{\frac{c\upsilon_\infty}{u_\infty}}$ and $RMn = Mn(cb)^2$. The constant or

$\varepsilon < 0$ represents that the wall is being heated or cooled respectively [28]. In the Equation (12),

$$Mn = \frac{M_0 B_0}{\rho_\infty u_\infty^2} \tag{15}$$

with $M_0 = \chi H_0, B_0 = \mu_0 H_0$.

The physical properties C_f (skin friction) and Nu (Nusselt number) are of primary interest whose are defined by the form

$$C_f = \frac{\tau_w}{\frac{1}{2}\rho_\infty u_\infty^2} \quad \text{and} \quad Nu = \frac{x q_w}{\kappa(T_0 - T_\infty)}$$

Where,

$$\tau_w = \left(\mu \frac{\partial u}{\partial y}\right)_{y=0} \quad \text{and} \quad q_w = -\kappa \left(\frac{\partial T}{\partial y}\right)_{y=0}.$$

Hence,

$$C_{f_x} = C_f \, \mathrm{Re}_x^{1/2} = \frac{2\theta_r}{(\theta_r - 1)} t''(\zeta, 0) \quad \text{and}$$

$$Nu_x = Nu \, \mathrm{Re}_x^{-1/2} = \left[1 + \frac{\varepsilon(\zeta - \zeta_i)(\zeta_j - \zeta)}{(\zeta_j - \zeta_i)^2}\right]^{-1} \theta'(\zeta, 0)$$

In Equation (14), $\theta(\zeta, 0)$ is the dimensionless wall temperature which is a continuous function with dimensionless stream wise distance ζ where ζ vary a small change with ζ_1 and ζ_2 over the constant value of 1. The introduction of a finite discontinuity at the leading and trailing edges of the slot when the wall temperature in the interval is increased or decreased by a constant value produces numerical challenges in the solution of the equations. To avoid this problem, we used a non-uniform distribution of wall temperature in the interval $[\zeta_i, \zeta_j]$ that varies slowly with ζ.

Where Pr Prandtl number, Mn magnetic number, θ_r viscosity parameter and S^* thermal conductivity parameter.

3 Numerical Scheme and Parameter Estimation

3.1 Numerical Method

In the current study, the governing problem is defined by a system of non-linear parabolic Equations (12)–(13) with boundary conditions (14) and is

numerically solved using a suitable technique. The velocity and the temperature profiles are the unknown functions. The numerical method used in this study with the principle of the common finite difference method with the use of central differences, tridiagonal matrix manipulation, and an iterative procedure. This methodology was developed by Kafoussias and Williams [18] and used in the studies of Tzirtzilakis and Kafoussias [19], and Murtaza et al. [26]. We first consider the first momentum equation and reduce its order, we get final ordinary differential equation in $F(x)$ defined by

$$F(x) = t'(\zeta, \eta), \text{ so that } F'(x) = t''(\zeta, \eta) \text{ and } F''(x) = t'''(\zeta, \eta) \tag{16}$$

Then we rewrite the Equation (12) assumes the form,

$$\begin{aligned} F''(x) - \frac{1}{2}t\frac{\theta-\theta_r}{\theta_r}F'(x) - \frac{\theta'}{\theta-\theta_r}\left[1+\frac{\varepsilon(\zeta-\zeta_i)(\zeta_j-\zeta)}{(\zeta_j-\zeta_i)^2}\right]^{-1}F'(x) \\ - \zeta\theta\left[1+\frac{\varepsilon(\zeta-\zeta_i)(\zeta_j-\zeta)}{(\zeta_j-\zeta_i)^2}\right]^{-1}\frac{\theta-\theta_r}{\theta_r} \\ = \zeta\frac{\theta-\theta_r}{\theta_r}\left(\frac{\partial t}{\partial\zeta}F'(x) - F(x)\frac{\partial t'}{\partial\zeta}\right) \\ \mp RMn\frac{(\zeta-ac)\zeta}{[(\zeta-ac)^2+(d\sqrt{\zeta}\eta-cb)^2]^2}\frac{\theta-\theta_r}{\theta_r} \end{aligned}$$

which can be rewritten as

$$\begin{aligned} F''(x) + \Bigg[-\frac{1}{2}t\frac{\theta-\theta_r}{\theta_r} - \frac{\theta'}{\theta-\theta_r}\left\{1+\frac{\varepsilon(\zeta-\zeta_i)(\zeta_j-\zeta)}{(\zeta_j-\zeta_i)^2}\right\}^{-1} \\ - \zeta\frac{\theta-\theta_r}{\theta_r}\frac{\partial t}{\partial\zeta}\Bigg]F'(x) + \zeta\frac{\theta-\theta_r}{\theta_r}\frac{\partial t'}{\partial\zeta}F(x) \\ = \zeta\theta\left[1+\frac{\varepsilon(\zeta-\zeta_i)(\zeta_j-\zeta)}{(\zeta_j-\zeta_i)^2}\right]^{-1}\frac{\theta-\theta_r}{\theta_r} \\ \mp RMn\frac{(\zeta-ac)\zeta}{[(\zeta-ac)^2+(d\sqrt{\zeta}\eta-cb)^2]^2}\frac{\theta-\theta_r}{\theta_r} \end{aligned} \tag{17}$$

This equation can be put as

$$p(x)F''(x) + q(x)F'(x) + r(x)F(x) = s(x) \tag{18}$$

in which

$$p(x) = 1, q(x) = -\frac{1}{2}t\frac{\theta-\theta_r}{\theta_r} - \frac{\theta'}{\theta-\theta_r}\left\{1+\frac{\varepsilon(\zeta-\zeta_i)(\zeta_j-\zeta)}{(\zeta_j-\zeta_i)^2}\right\}^{-1} - \zeta\frac{\theta-\theta_r}{\theta_r}\frac{\partial t}{\partial\zeta}, r(x) = \zeta\frac{\theta-\theta_r}{\theta_r}\frac{\partial t'}{\partial\zeta},$$

$$s(x) = \zeta\theta\left[1+\frac{\varepsilon(\zeta-\zeta_i)(\zeta_j-\zeta)}{(\zeta_j-\zeta_i)^2}\right]^{-1}\frac{\theta-\theta_r}{\theta_r} \mp RMn\frac{(\zeta-ac)\zeta}{[(\zeta-ac)^2+(d\sqrt{\zeta}\eta-cb)^2]^2}\frac{\theta-\theta_r}{\theta_r}$$

In a similar manner, Equation (13) which is already linear can be put in the form of (18) as

$$\frac{1}{\mathrm{Pr}}(1+S^*\theta)\theta'' + \left(\frac{1}{\mathrm{Pr}}S^*\theta' + \frac{1}{2}t\right)\theta' + \zeta\frac{\partial t}{\partial\zeta}\theta' = \zeta t'\frac{\partial\theta}{\partial\zeta}$$

This equation can be further written as

$$\frac{1}{\mathrm{Pr}}(1+S^*\theta)\theta'' + \left(\frac{1}{\mathrm{Pr}}S^*\theta' + \frac{1}{2}t + \zeta\frac{\partial t}{\partial\zeta}\right)\theta' = \zeta t'\frac{\partial\theta}{\partial\zeta} \tag{19}$$

Set $F(x) = \theta(\zeta, \eta)$, we get

$$p(x)F''(x) + q(x)F'(x) + r(x)F(x) = s(x) \tag{20}$$

Where

$$p(x) = \frac{1}{\mathrm{Pr}}(1+S^*\theta), q(x) = \frac{1}{2}t + \frac{1}{\mathrm{Pr}}S^*\theta' + \zeta\frac{\partial t}{\partial\zeta}, r(x) = 0 \quad \text{and}$$

$$s(x) = \zeta t'\frac{\partial\theta}{\partial\zeta}.$$

To solve the system under consideration, the numerical scheme consists of proceeding in the ζ-direction. The previous iterations at ζ_i are known in order to calculate unknown profiles at ζ_{i+1}. The process starts at $\zeta = 0$, where the Equations (12) and (19) reduce to

$$t''' - \frac{1}{2}t\frac{\theta-\theta_r}{\theta_r}t'' - \frac{\theta'}{\theta-\theta_r}\left[1-\frac{\varepsilon\zeta_i\zeta_j}{(\zeta_j-\zeta_i)^2}\right]t'' = 0 \tag{21}$$

and

$$\frac{1}{\mathrm{Pr}}(1+S^*\theta)\theta'' + \left(\frac{1}{\mathrm{Pr}}S^*\theta' + \frac{1}{2}t\right)\theta' = 0 \tag{22}$$

The boundary conditions of (21)–(22) are provided in (14) and the numerical solutions of (21) and (22) with (14) is determined by using an effective numerical technique based on the conversion of the equations in the form of (18) and (20).

To find from ζ_i to ζ_{i+1}, the equations are discretized at $\zeta_{i+\frac{1}{2}}, \eta_j$ with central differences for backward differences for first order ζ-derivative sand for first and second order derivatives. The numerical technique of Crank-Nicolson is implemented on a uniform (ζ, η) grid. Equation (13) gives $\theta_{i+1,j}$ utilizing a fast-tridiagonal technique after an estimate of unknown $t'_{i+1,j}$ is provided. This profile is used to solve (12), iteratively based on tridiagonal technique and obtained $t'_{i+1,j}$. The procedure is revisited till the desired result at ζ_{i+1} is obtained. In this problem we use the discretization steps $\Delta\zeta = 0.001$, $\Delta\eta = 0.6$ and consider the value of $\eta_\infty = 10.0$ according to the final ζ-station. The current and prior iterations are compared using a convergence condition based on the comparative variance. When this dissimilarity reaches at 10^{-6}, the solution is said to have converged, and the iterative procedure is completed.

3.2 Parameter Estimation

Numerical computations for the dimensionless parameters involved in this problem have been performed. Here dimensionless ratio $\zeta(x) = \frac{Gr_x}{\mathrm{Re}_x^2}$ represents the types of flow. We found different type of convection such as $\zeta \ll 1$ means forced convection, $(\zeta \sim 1)$ then it is mixed convection and $(\zeta \gg 1)$ for free convection. The maximum value of ζ determined to 0.5(*x-final* $= 0.76$) for this study.

Blood is the biomagnetic fluid in this case the density is $\rho_\infty = 1050$ kgm^{-3}, viscosity is $\mu_\infty = 3.2 \times 10^{-3}$ kgm^{-1} s^{-1}, the free stream velocity is $u_\infty = 0.28$ ms^{-1} (cf. [22]). The temperature of the vertical plate is $T_0 = 45^\circ\mathrm{C} = 318$ K and the blood temperature in the free stream is $T_\infty = 15^\circ\mathrm{C} = 288$ K. As a result, the temperature difference is $\Delta T = T_0 - T_\infty = 30$ K. For these temperatures, specific heat under constant pressure $c_p = 4 \times 10^3$ JKg^{-1} K^{-1} and thermal conductivity $\kappa_\infty = 0.6$ Jm^{-1} s^{-1} K^{-1} are used as measures for blood (cf. [25]). Although μ, c_p, κ of any fluid, and hence of the blood, are usually independent of temperature, the Prandtl number Pr can be

considered constant. Thus [16, 19]

$$\Pr = \frac{\mu_\infty c_p}{\kappa_\infty} = \frac{3.2 \times 10^{-3}\ \mathrm{Kgm^{-1}\ s^{-1}} \times 4 \times 10^3\ \mathrm{JKg^{-1}\ K^{-1}}}{0.6\ \mathrm{Jm^{-1}\ s^{-1}\ K^{-1}}} \approx 21.0$$

The thermal expansion coefficient of blood is $\beta = 0.18 \times 10^{-3}\ \mathrm{K^{-1}}$ and $g = 9.81\ \mathrm{ms^{-2}}$ [22]. Under these conditions, the constant c, specified in Equation (7), produces the value $c = 0.662$. Assume that the electric wire is positioned at the point $(x_0, y_0) = (a, b) = (0.50, -0.20)$. In the converted and dimensionless coordinate system $O\zeta\eta$, the position of the wire is $(\zeta_0, \eta_0) = (0.331, -85.73)$.

For liquids, the viscosity parameter θ_r takes negative values for positive temperature difference $\Delta T = T_0 - T_\infty$. The values of θ_r are taken equal to $\theta_r = -0.40, -0.50$ and -0.60 [22] and thermal conductivity parameter S^* is taken to be equal to $S^* = 0.14$ for the specified temperature difference. For $B_0 = 1.2$ T and $M_0 = 40\ \mathrm{Am^{-1}}$ [27], the value of Mn is

$$Mn = \frac{M_0 B_0}{\rho_\infty u_\infty^2} = \frac{40\ \mathrm{Am^{-1}} \times 1.2\ \mathrm{T}}{1050\ \mathrm{Kgm^{-3}} \times (0.28\ \mathrm{ms^{-1}})^2} = 0.6$$

The electrical conductivity of blood can be considered minimal with the value of $B_0 = 1.2$ T. The situation $Mn = 0.0$ represents blood flow in the absence of a magnetic field.

4 Results and Discussion

For numerous parameters of this problem $Mn, \theta_r, \zeta, \varepsilon, \Pr$ and S^* the converted Equations (12) and (13) with (14) are numerically solved using the finite-difference scheme. The range of parameter values we have used for numerical computations are: $-0.40 \le Mn \le 0.60, 0 \le \zeta \le 0.5, -0.25 \le \varepsilon \le 0.25, \Pr = 21.0$ and $S^* = 0.0, 0.14$. It may be noted that for the purpose of computation, we take a slot located in the interval $[\zeta_i, \zeta_j] = [0.1, 0.3]$ [28]. The wall is heated or cooled in this specified interval. The temperature $T_0(T_\infty)$ of the remaining part of the wall remains constant.

Figures 2 and 3 represent the accuracy of our method by comparing the velocity profile $t'(\zeta, \eta)$ and temperature profile $\theta(\zeta, \eta)$ for $\varepsilon = 0, \Pr = 21.0, \theta_r = -0.50, Mn = 0.40, \zeta = 0.24$ setting $\eta_{\max} = 10.0$ and 2.5 with those reported in [22]. The results with $\varepsilon = 0$ are found to be in very good agreement (cf. Figure 2).

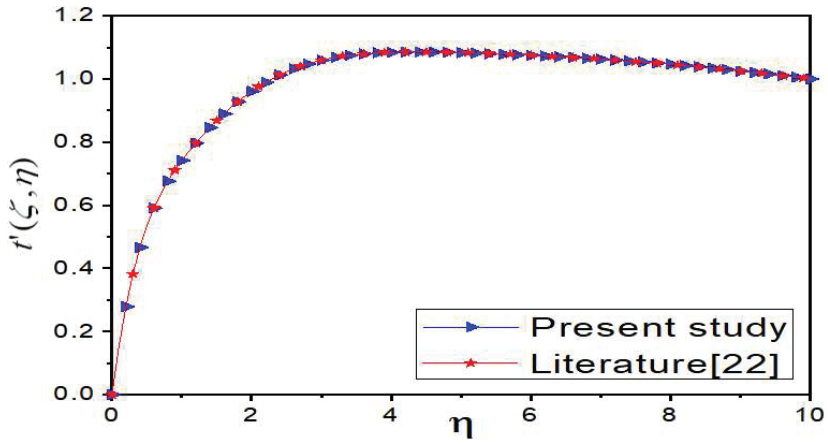

Figure 2 Comparison of dimensionless velocity $t'(\zeta, \eta)$.

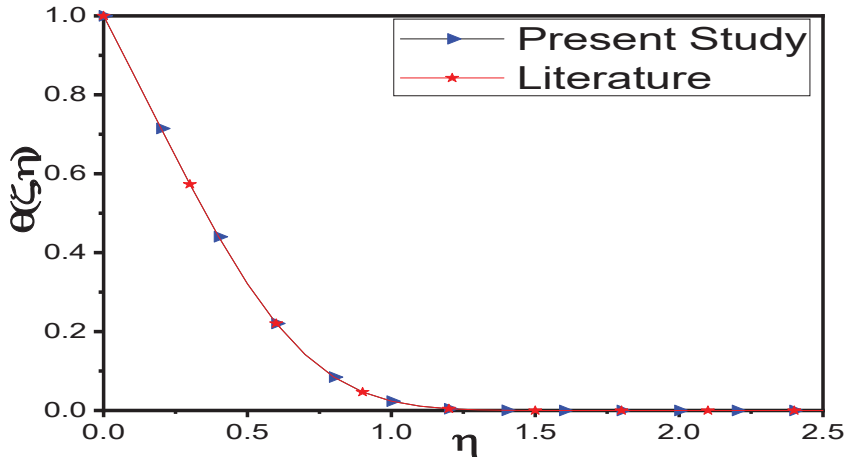

Figure 3 Comparison of dimensionless temperature $\theta(\zeta, \eta)$.

The space change of the velocity profile $t'(\zeta, \eta)$ and the temperature profile $\theta(\zeta, \eta)$, for $\theta_r = -0.50, \zeta = 0.24, \varepsilon = 0.25$ and -0.25 for various assessments of the magnetic number $Mn = 0.10, 0.20, 0.40, 0.50$ are presented in Figures 4 and 5, respectively.

In Figure 4, the effect of wall heating ($\varepsilon = 0.25$) and wall cooling ($\varepsilon = -0.25$) on the velocity field is found to be negligible. The velocity profile starts from $t'(\zeta, 0) = 0$ and increases to the boundary value $t'(\zeta, 5.0) = 1$ for all ζ.

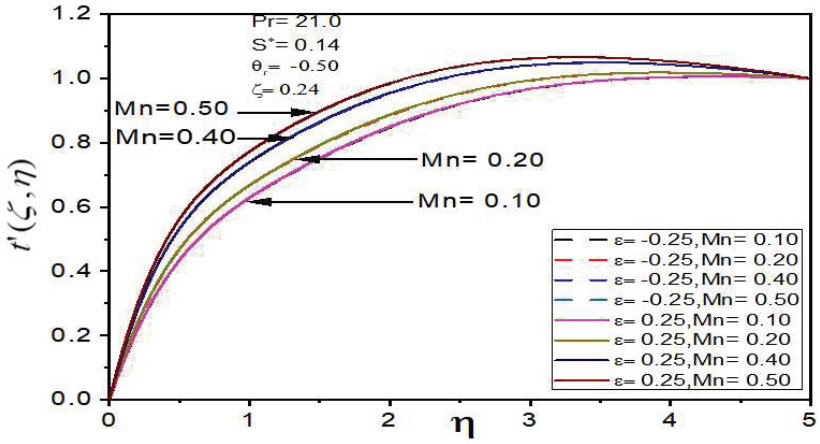

Figure 4 Velocity profile $t'(\zeta, \eta)$ for different magnetic number, wall heating $(\varepsilon = 0.25)$ and wall cooling $(\varepsilon = -0.25)$.

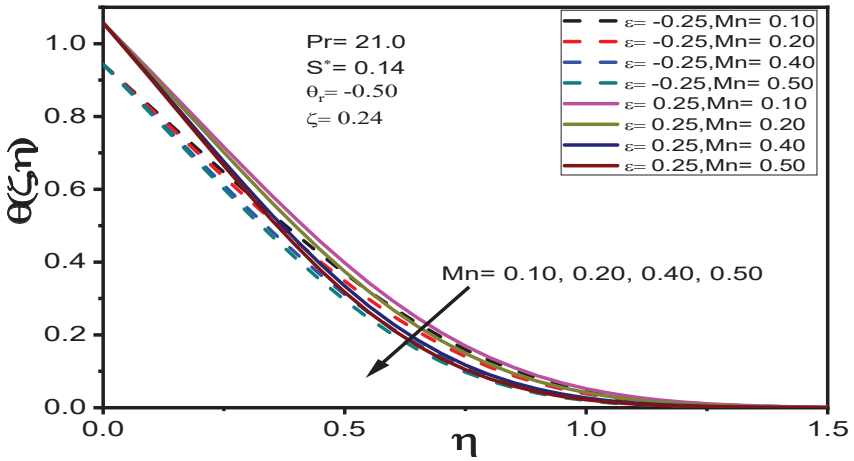

Figure 5 Temperature profile $\theta(\zeta, \eta)$ for different magnetic number Mn, wall heating $(\varepsilon = 0.25)$ and wall cooling $(\varepsilon = -0.25)$.

In Figure 5, the temperature profile starts from $(0, 1.0569)$ for wall heating $(\varepsilon = 0.25)$, while it starts from $(0, 0.9431)$ for wall cooling $(\varepsilon = -0.25)$. In both the cases the temperature profile decreases gradually and ends at the boundary layer.

From Figures 4 and 5 it is concluded that, for every value of ζ, velocity increases with magnetic number Mn whereas reverse trend show for temperature profile.

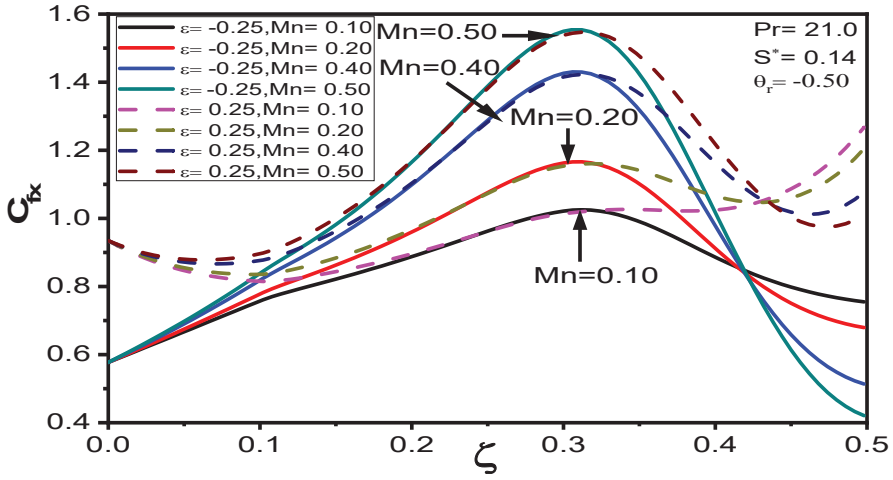

Figure 6 Skin friction coefficient C_{f_x} for different magnetic numbers Mn for the cases of wall heating ($\varepsilon = 0.25$) and wall cooling ($\varepsilon = -0.25$).

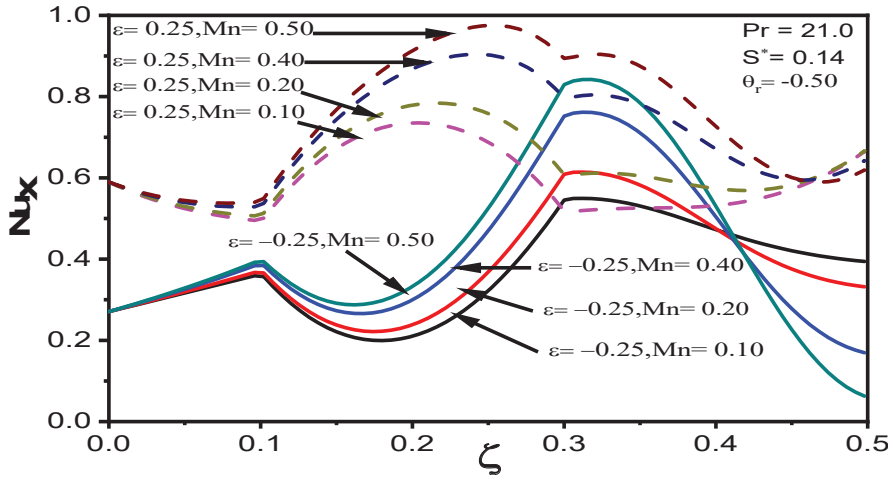

Figure 7 Variations of Nusselt number Nu_x for various values of magnetic number Mn, for the case of wall heating ($\varepsilon = 0.25$) and wall cooling ($\varepsilon = -0.25$).

Figures 6 and 7 show the space variations of the dimensionless skin friction coefficient C_{f_x} and the Nusselt number Nu_x with ζ, for $\theta_r = 0.50$ and $Mn = 0.10, 0.20, 0.40, 0.50$, respectively.

In Figure 6, the skin friction coefficient starts from $(0, 0.9347)$ and decreases slightly in the slot $[0, 0.1]$ for wall heating ($\varepsilon = 0.25$) and then

increases rapidly with the dimensionless distance ζ. Again, the skin friction coefficient starts from $(0, 0.5773)$ and increases gradually for wall cooling $(\varepsilon = -0.25)$. The skin friction coefficients for both cases agree in the slot $[0.1, 0.3]$. The skin frictions for both cases are influenced by the existence of the different magnetic field and take their supreme value in the region denoted by $\zeta = 0.3$. Beyond $\zeta = 0.3$, the skin friction coefficients decrease for both cases and intersect at $(0.432, 1.0607)$ for wall heating and intersect at $(0.42, 0.84)$ for wall cooling. Beyond the point of intersection, the skin friction coefficient induced in the case of wall heating and decreases for wall cooling.

From Figure 7 it is seen that the Nusselt number starts from $(0, 0.5899)$, increases in a rectilinear manner in the interval $[0, 0.1]$ and then the graphs are convex upwards in the interval $[0.1, 0.3]$ for wall heating $(\varepsilon = 0.25)$. The Nusselt number also starts from $(0, 0.2709)$ and increases linearly in the slot $[0, 0.1]$ and then concave downwards in the slot $[0.1, 0.3]$ for wall cooling $(\varepsilon = -0.25)$. The impact of wall heating and cooling parameter show the reverse behavior on the Nusselt number in the slot $[0.1, 0.3]$, but for the wall cooling we see it is not a mirror reflection. Beyond $\zeta = 0.3$, a little far upstream the Nusselt numbers of different magnetic numbers intersect at $(0.462, 0.5909)$ for wall heating and a little far downstream the Nusselt numbers of different magnetic numbers intersect at $(0.414, 0.4411)$ for wall cooling. Beyond the point of intersection, the Nusselt number increases for wall heating and decreases for wall cooling.

It may be noted that, the influence of heating $(\varepsilon = 0.25)$ and cooling $(\varepsilon = -0.25)$ in the interval $[\zeta_i, \zeta_j] = [0.1, 0.3]$ are more noticeable on the Nusselt number (Nu_x) than the coefficient of skin friction (C_{f_x}), because the wall heating/cooling parameter directly impact the thermal field.

Figures 8 and 9 show the space variation of the velocity and temperature profiles, respectively, for $Mn = 0.40, \theta_r = -0.50$ and at different positions ζ through a vertical plate.

In Figure 8, it is observed that in the interval $[0.0, 0.36]$ for ζ increases, the fluid velocity profile $t'(\zeta, \eta)$, like the axis or plate inside the thin layer and accelerates, from the initial value zero, on the wall, to the free stream velocity. It is also find that forced convection dominates for the leading edge near the plate ($\zeta = 0.0$ or $\zeta = 0.12$), but for as ζ increases ($\zeta = 0.24$ or $\zeta = 0.36$) the convection transfers into the mixed area and consequently into a free convective regime. So, buoyancy-force performance along free stream and velocity within thin layer can approximated the outer value $t'(\zeta, \infty) = 1$ showing a possible overshoot in it $(t'(\zeta, \eta) > 1)$. It is observed that the effect

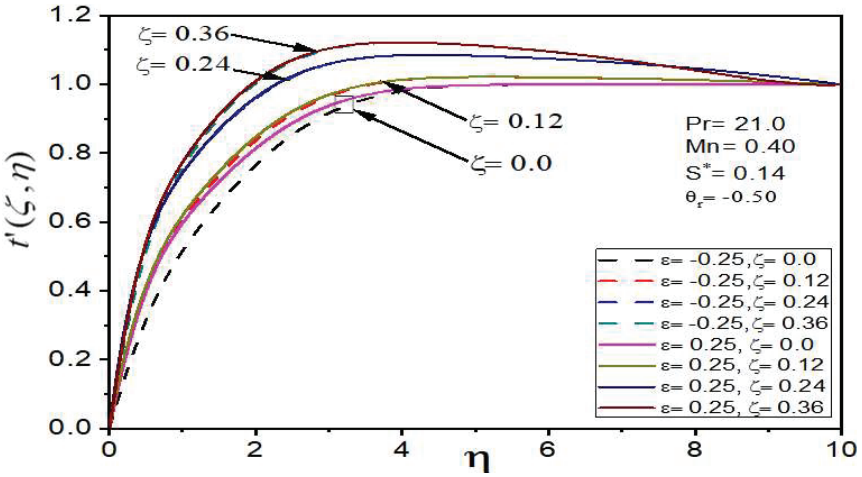

Figure 8 Velocity profile $t'(\zeta, \eta)$ at different places ζ and for wall heating $(\varepsilon = 0.25)$ and wall cooling $(\varepsilon = -0.25)$.

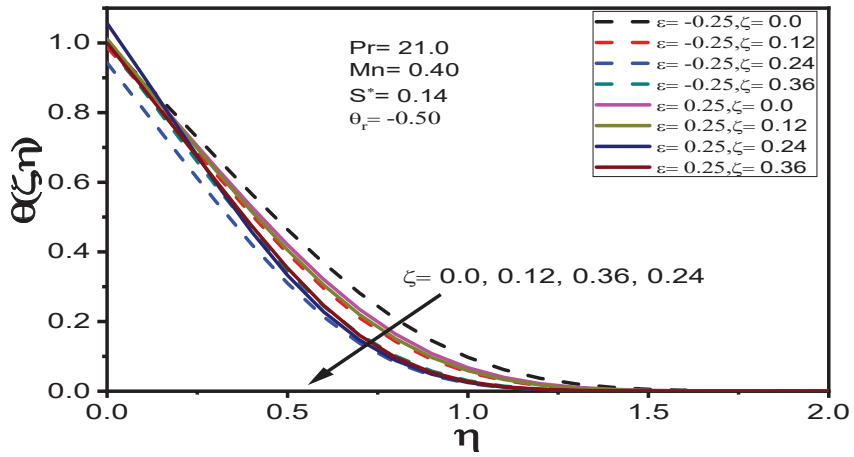

Figure 9 $\theta(\zeta, \eta)$ for various values of ζ, in the case of wall heating $(\varepsilon = 0.25)$ and wall cooling $(\varepsilon = -0.25)$.

of wall heating $(\varepsilon = 0.25)$ and wall cooling $(\varepsilon = -0.25)$ is much less for $\zeta = 0.0$ and negligible for other values of ζ.

In Figure 9, as ζ increases, the dimensionless temperature $\theta(\zeta, \eta)$ decreases except for the value $\zeta = 0.36$ inside the thermal boundary layer. At the place $\zeta = 0.36$, the temperature, for all η, is enhanced than that of the corresponding $\zeta = 0.24$. At $\zeta = 0.0, 0.36$ the dimensionless temperature

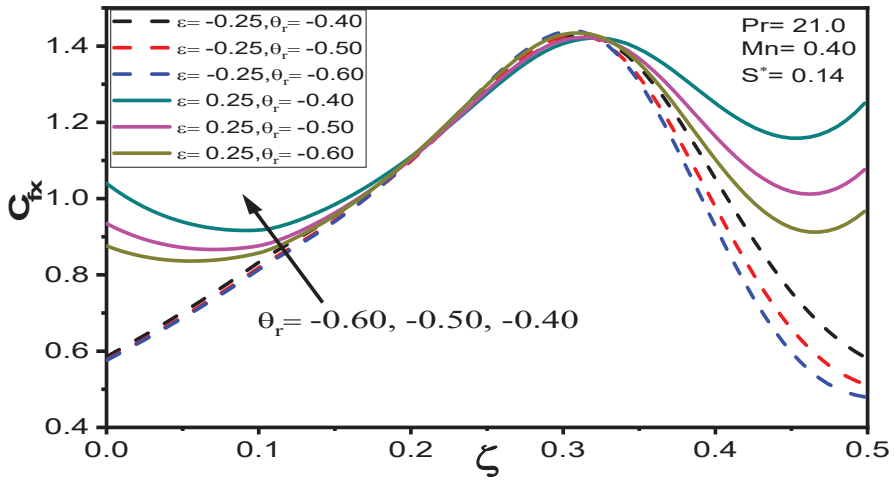

Figure 10 Change in skin friction coefficient (C_{f_x}) for different values of viscosity/temperature parameter θ_r.

starts from $(0, 1)$ and ends at the boundary layer at the free stream for wall heating $(\varepsilon = 0.25)$ and wall cooling $(\varepsilon = -0.25)$, respectively. At $\zeta = 0.12$ the dimensionless temperature reaches at $(0, 1.0119)$ for wall heating and reaches at $(0, 0.9881)$ for wall cooling. At $\zeta = 0.24$ the dimensionless temperature reaches at $(0, 1.0569)$ for wall heating and reaches at $(0, 0.9431)$ for wall cooling.

Figures 10 and 11 represent the space variations of the skin friction coefficient (C_{f_x}) and Nusselt number (Nu_x) and for different values of the viscosity/temperature parameter θ_r when $Mn = 0.40$. It is known that when $|\theta_r|$ is large, the variation of viscosity parameter on the boundary layer is negligible but for $\theta_r < 0$, the viscosity variation play an important role.

Figure 10 shows that the skin friction coefficient is reduced slightly in the interval $[0, 0.1]$ but it increases gradually in $[0.1, 0.3]$ as $|\theta_r|$ decreases for wall heating $(\varepsilon = 0.25)$. The change in the skin friction coefficient for wall cooling $(\varepsilon = -0.25)$ is rather less. The impact of the wall cooling $(\varepsilon = -0.25)$ on the skin friction coefficient is very similar to the wall heating in the interval $[0.1, 0.3]$. The graphs for skin friction coefficients for both the cases intersect at $(0.324, 1.4248)$. Beyond this point, the skin friction coefficient reduces in both cases. After a downstream, the skin friction coefficient slightly upstream for wall heating.

From Figure 11, one may observe that the Nusselt number decreases slightly in $[0, 0.1]$ and convex upwards in $[0.1, 0.3]$, then slightly upstream as

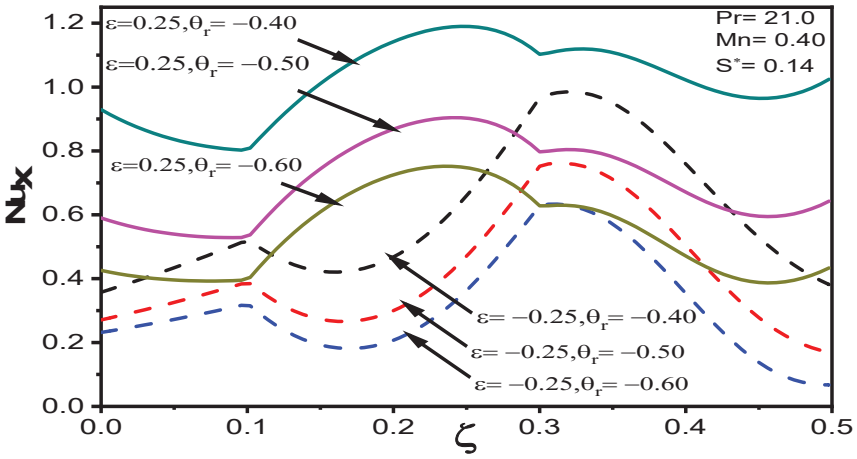

Figure 11 Variation of Nusselt number (Nu_x) for different values of viscosity/temperature parameter θ_r.

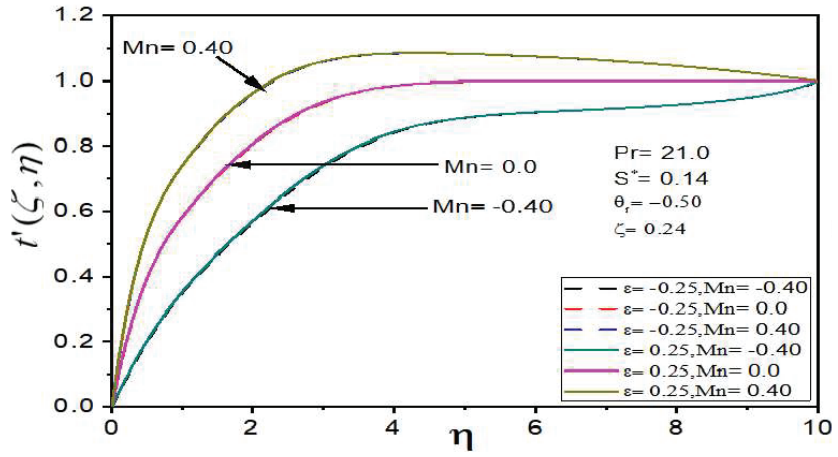

Figure 12 Change in velocity profile $t'(\zeta, \eta)$ for positive, negative and zero values of Mn.

$|\theta_r|$ decreases for wall heating. Also, the Nusselt number increases linearly in $[0, 0.1]$ and concave downwards in the slot $[0.1, 0.3]$ and then decreases gradually in the case of wall cooling $(\varepsilon = -0.25)$. The impact of wall heating on the Nusselt number is of opposite type to that of the wall cooling in $[0.1, 0.3]$.

Figures 12 and 13 represent velocity profile $t'(\zeta, \eta)$ and temperature profile $\theta(\zeta, \eta)$, for $\zeta = 0.24, \theta_r = -0.50$ and for $Mn = 0.0, \pm 0.40$.

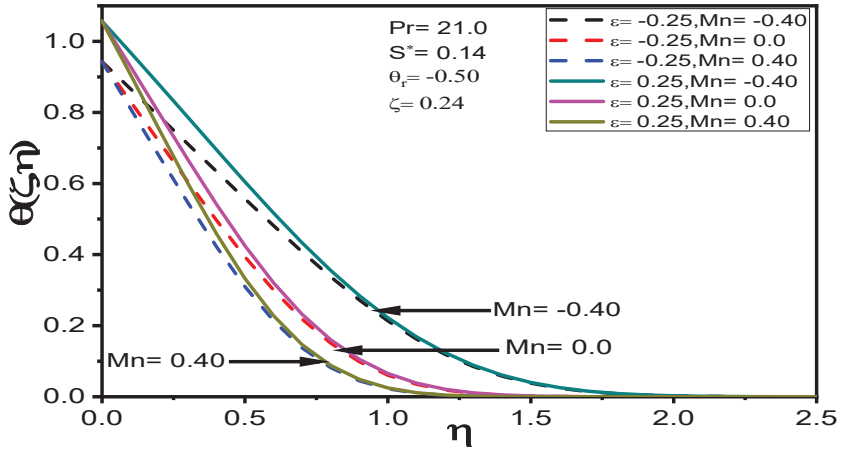

Figure 13 Change in the temperature profile $\theta(\zeta, \eta)$ when $Mn > 0, < 0$ and $= 0$ in the cases of wall heating/cooling.

From Figure 12, we find that when $Mn = 0.0, -0.40$, the change in the velocity profile is greater than that when it changes between from 0.0 to 0.40. The effect of the wall heating $(\varepsilon = 0.25)$ and wall cooling $(\varepsilon = -0.25)$ on the velocity field is not very appreciable. The velocity profile increases significantly in the boundary layer, increases from zero on the plate to its limiting value 1, at the free stream.

Figure 13 revealed that when Mn changes from 0.0 to -0.40, the change in the temperature profile is greater than that when the Mn changes from 0.0 to 0.40. The temperature profile starts from $(0, 1.0569)$ for wall heating $(\varepsilon = 0.25)$ and it starts from $(0, 0.9431)$ in the case of wall cooling $(\varepsilon = -0.25)$. The temperature profile diminishes in a gradual manner in the boundary layer for both the cases.

Spatial variations of the skin friction coefficient (C_{f_x}) and the Nusselt number Nu_x, are shown for various Mn in Figures 14 and 15, when $\theta_r = -0.50$.

Figure 14 shows that the skin friction coefficient starts from $(0, 0.9437)$ and it decreases slightly in $[0, 0.1]$ for wall heating $(\varepsilon = 0.25)$. Beyond $\zeta = 0.1$, as ζ increases, the skin friction coefficient for wall heating gradually increases for $Mn = 0.40$ but it gradually decreases for $Mn = -0.40$. The skin friction coefficient for wall cooling $(\varepsilon = -0.25)$ also starts from $(0, 0.5773)$ and increases rapidly for $Mn = 0.40$ and decreases for $Mn = -0.40$. We see that when $Mn = 0.40$, C_{f_x} attains its maximum position at $\zeta = 0.312$ and minimum at $\zeta = 0.288$ for $Mn = -0.40$.

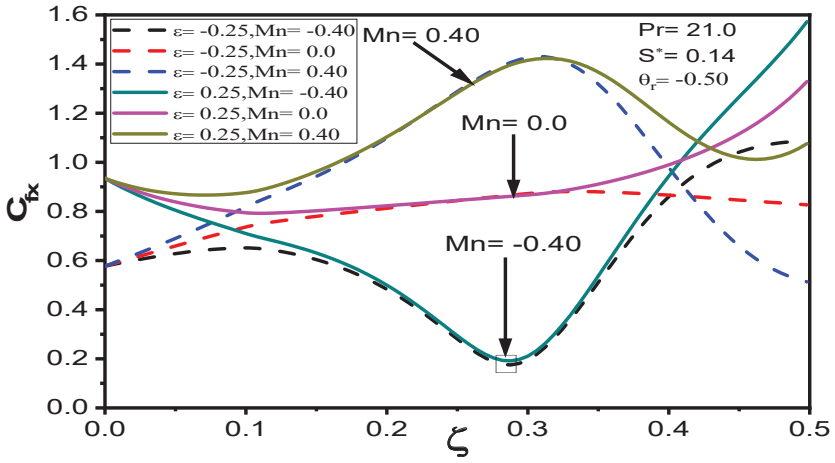

Figure 14 Skin friction coefficient C_{f_x} with ζ for Mn.

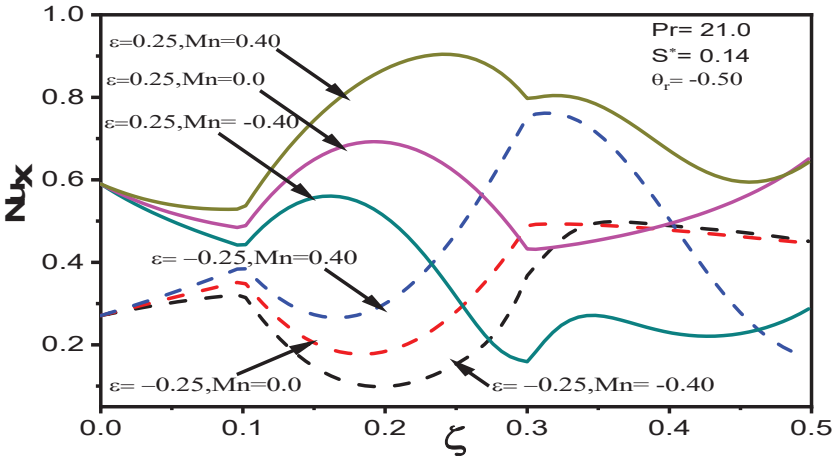

Figure 15 Variations of the dimensionless Nusselt number Nu_x for positive, negative and zero magnetic number Mn.

The plots for skin friction coefficient for $Mn = 0.40$ and $Mn = -0.40$ intersect at $(0.42, 1.0865)$ in the case of wall heating, while the plots for skin friction coefficient for $Mn = 0.40$ and $Mn = -0.40$ also intersect at $(0.408, 0.9195)$, when wall cooling takes place.

In Figure 15 shows that the plot for the Nusselt number starts from $(0, 0.5899)$ and decreases linearly in $[0, 0.1]$ in the case of wall heating $(\varepsilon = 0.25)$. In the case of wall cooling, the plot starts from $(0, 0.2709)$ and

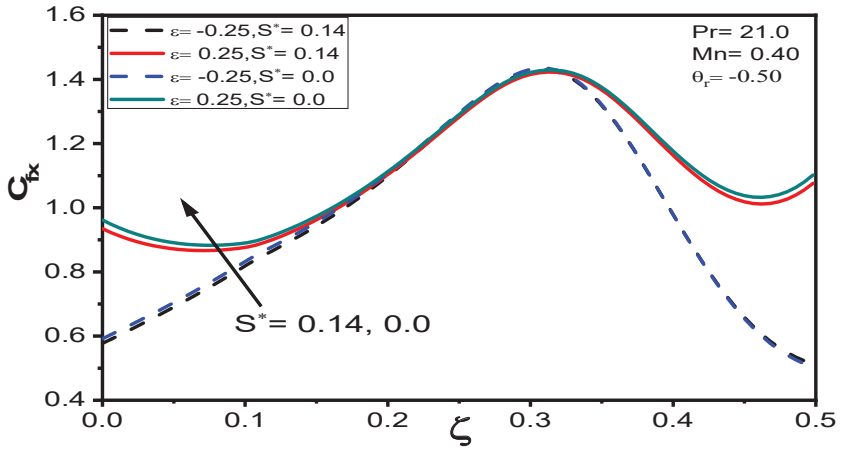

Figure 16 Distribution of skin friction coefficient C_{f_x} for various values of S^* for the cases of wall heating ($\varepsilon = 0.25$) and wall cooling ($\varepsilon = -0.25$).

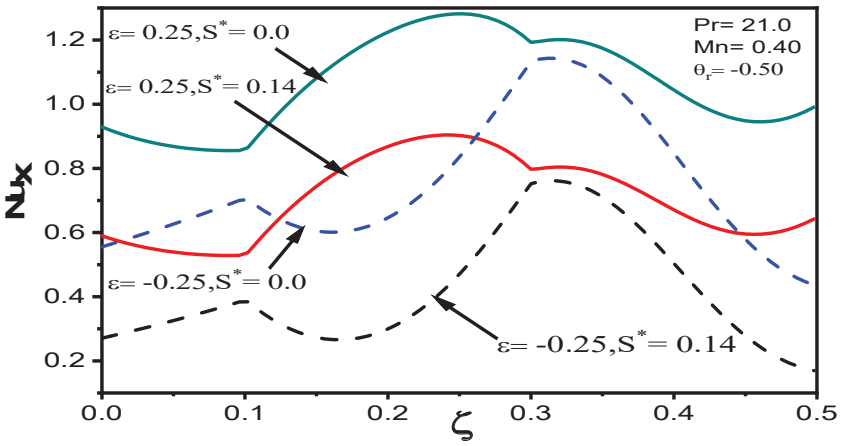

Figure 17 Spatial variations of Nusselt number Nu_x for altered values of thermal conductivity parameter S^*.

increases linearly in $[0, 0.1]$ for wall cooling. In $[0.1, 0.3]$ the Nusselt number is convex upwards for wall heating and concave downwards for wall cooling. The effect of the wall heating is of a reverse nature in the case of wall cooling in $[0.1, 0.3]$.

Figures 16 and 17 present the variations of the skin friction coefficient C_{f_x} and the Nusselt number Nu_x, vs ζ for $\theta_r = -0.50, Mn = 0.40$ and varying S^* respectively.

From Figure 16, we find that the skin friction coefficient decreases slightly in $[0, 0.1]$, then increases in $[0.1, 0.3]$ and finally diminishes significantly for wall heating ($\varepsilon = 0.25$). The skin friction coefficient for wall cooling ($\varepsilon = -0.25$) increases from the leading edge and it attains a maximum at $\zeta = 0.3$. Starting from the point $(0.3, 1.4289)$ the skin friction coefficient diminishes gradually.

In Figure 17, we find that the Nusselt number decreases linearly in $[0, 0.1]$, convex upwards in $[0.1, 0.3]$ and slightly upstream in the case of wall heating. In the case of wall cooling, however, the Nusslt number increases linearly in $[0, 0.1]$, concave downwards in $[0.1, 0.3]$ and finally decreases linearly. The reverse behavior shown for the Nusselt number for different value of wall parameter (heating or cooling) in $[0.1, 0.3]$.

5 Conclusions

A numerical analysis of steady viscous two-dimensional laminar incompressible boundary layer flow with mixed convective on the biomagnetic fluid above a vertical plate under the action of an applied magnetic field and localized heating/cooling has been performed in this work. The momentum and energy equations were reduced to nonlinear coupled partial differential equations using a similarity transformation. The governing problem in the form of partial differential equations have been solved by a new technique with the finite difference method. The impacts of the dimensionless parameters $\mathrm{Pr}, Mn, \theta_r, \zeta, \varepsilon$ and S^* on the fluid flow have been discussed. To validate the study, the numerical results obtained have been compared with the results of previous study reported earlier in scientific literatures and they are found to be in good agreement. Significant results of the study regarding the variations of fluid properties lead to the following conclusions:

1. Changes in velocity and temperature profiles at every location of the vertical plate depend quit significantly on the magnetic properties.
2. The existence of a magnetic field has a significant impact on skin-friction and Nusselt number. The effect is more pronounced when the magnetic field intensity is high. The effects of wall parameter (heating or cooling) are more prominent for Nusselt number than for the skin friction.
3. For both physical parameter, enhancing the sensitivity of the viscosity parameter to temperature via the parameter θ_r has a considerable effect. The skin friction and the Nusselt number both decrease as $|\theta_r|$ increases.

4. In the case of $Mn < 0$, the impact of Mn on the flow field is qualitatively and quantitatively different from the situation of $Mn > 0$.

The findings of the study are believed to be quit useful to clinicians for having a better insight of blood flow in arteries, when the human body is subject to a magnetic field.

References

[1] Alimohamadi, H., and Sadeghy, K. (2015). On the use of magnetic fields for controlling the temperature of hot spots on porous plaques in stenosis arteries. Nihon Reoroji Gakkaishi, 43(5), 135–144.

[2] Misra, J. C., Sinha, A., and Shit, G. C. (2010). Flow of a biomagnetic viscoelastic fluid; application to estimate of blood flow in arteries during electromagnetic hyperthermia, a therapeutic procedure for cancer treatment. Applied Mathematics in Mechanical Engineering, 31(11), 1405–1420.

[3] Haik, Y., Pai, V., and Chen, C. J. (1999). Development of magnetic device for cell separation. Journal of Magnetism and Magnetic Materials, 194(1–3), 254–261.

[4] Higashi, T., Yamagishi, A., Takeuchi, T., Kawaguchi, N., Sagawa, S., Onishi, S., et al. (1993). Orientation of erythrocytes in a strong static magnetic field. Blood, 82(4), 1328–1334.

[5] Gasparovic, C., and Matweiyoff, N. A. (1992). The magnetic properties and water dynamics of the red blood cell. Magnetic Resonance in Medicine, 26(2), 274–299.

[6] Higashi, T., Ashida, N., and Takeuchi, T. (1997). Orientation of blood cells in static magnetic field. Physica B: Condensed Matter, 237, 616–620.

[7] Pauling, L., and Coryell, C. D. (1936). The magnetic properties and structure of hemoglobin, oxyhemoglobin and carbonmonoxy hemoglobin. Proceedings of the National Academy of Science of the United States of America, 22(4), 210–216.

[8] Motta, M., Haik, Y., Gandhari, A., and Chen, C. J. (1998). High magnetic field effects on human deoxygenated hemoglobin light absorption. Bioelectrochemistry and Bioenergetics, 47(2), 297–300.

[9] Alam, J., Murtaza, M. G., Tzirtzilakis, E. E., and Ferdows, M. (2022). Mixed convection flow and heat transfer of Biomagnetic fluid with magnetic/non-magnetic particles due to a stretched cylinder in the

presence of a magnetic dipole. *Proceedings of International Exchange and Innovation Conference on Engineering & Sciences (IEICES), 8*, 76–83.

[10] Ruuge, E. K., and Rusetski, A. N. (1993). Magnetic fluids as drug carriers: targeted transport of drugs by a magnetic field. Journal of Magnetism and Magnetic Materials, 122(1–3), 335–339.

[11] Lauva, M., and Plavins, J. (1993). Study of colloidal magnetic binding erythrocytes: prospects for cell separation. Journal of Magnetism and Magnetic Materials, 122, 349–353.

[12] Haik, Y., Pai, V., and Chen, C. J. (1999). Biomagnetic fluid dynamics. Cambridge University Press, 439–452.

[13] Haik, Y., Chen, J. C., and Pai, V. M. (1996, June 25–28). Development of biomagnetic fluid dynamics. In: Proceedings of the IX International Symposium on Transport Properties in Thermal Fluid Engineering, Singapore. Pacific Center of Thermal Fluid Engineering, pp. 121–126.

[14] Rosensweig, R. E. (1987). Magnetic fluids. Annual Review of Fluid Mechanics, 19, 437–461.

[15] Tzirtzilakis, E. E. (2006, July 10–14). A mathematical model for blood flow in magnetic field. International Symposium on Trends in Applications of Mathematics to Mechanics (STAMM 2006), Vienna, Austria.

[16] Murtaza, M. G., Tzirtzilakis, E. E., and Ferdows, M. (2017). Effect of electrical conductivity and magnetization on the biomagnetic fluid flow over a stretching sheet. Journal of Applied Mathematics and Physics, 68, 93.

[17] Ferdows, M., Alam, J., Murtaza, G., Tzirtzilakis, E. E., and Sun, S. (2022). Biomagnetic flow with $CoFe_2O_4$ magnetic particles through an unsteady stretching/shrinking cylinder. *Magnetochemistry*, 8, 27.

[18] Kafoussias, N. G., and Williams, E. W. (1999). An improved approximation technique to obtain numerical solution of a class of two-point boundary value similarity problems in fluid mechanics. International Journal for Numerical Methods in Fluid, 17(2), 145–162.

[19] Tzirtzilakis, E. E., and Kafoussias, N. G. (2003). Biomagnetic fluid flow over a stretching sheet with nonlinear temperature dependent magnetization. Zeitschriftfur Angewandte Mathematik and Physik, 54(4), 551–565.

[20] Tzirtzilakis, E. E., Xenos, M., Loukopoulos, V. C., and Kafoussias, N. G. (2006). Turbulent biomagnetic fluid flow in a rectangular channel

under the action of a localized magnetic field. International Journal of Engineering Science, 44(18–19), 1205–1224.

[21] Fukada, E., and Kaibara, M. (1980). Viscoelastic study of aggregation of red blood cells. Biorheology, 17(1–2), 177–182.

[22] Kafoussias, N. G., Raptis, A., and Tzirtzilakis, E. E. (2008). Free-forced convective boundary layer flow of a biomagnetic fluid under the action of a localized magnetic field. Canadian J. of Physics, 86, 447–457.

[23] Stoltz, J. F., and Lucius, M. (1981). Viscoelasticity and thixotropy of human blood. Biorheology, 18(3–6), 453–473.

[24] Thurston, G. B. (1972). Viscoelasticity of human blood. Biophysical Journal, 12(9), 1205–1217.

[25] Tzirtzilakis, E. E., Kafoussias, N. G., and Raptis, A. (2010). Numerical study of forced and free convective boundary layer flow of a magnetic fluid over a flat plate under the action of alocalized magnetic field. ZAMP, 929–947.

[26] Murtaza, M. G., Tzirtzilakis, E. E., and Ferdows, M. (2018). Numerical solution of three dimensional unsteady biomagnetic flow and heat transfer through stretching/shrinking sheet using temperature dependent magnetization. Archives of Mechanics, 70(2), 161–185.

[27] Merkin, J. H., and Mahmood, T. (1989). Mixed convection boundary layer similarity solution. Prescribed wall heat flux. ZAMP, 40, 61–68.

[28] Chamkha, A. J., Takhar, H. S., and Nath, G. (2004). Mixed convection flow over a vertical plate with localized heating (cooling), magnetic field and suction (injection). Heat and Mass Transfer, 40, 835–841.

[29] Loukopoulos, V. C., and Tzirtzilakis, E. E. (2004). Biomagnetic channel flow in spatially varying magnetic field. International Journal of Engineering Science, 42, 571–590.

[30] Alam, J., Murtaza, M. G., Tzirtzilakis, E. E., and Ferdows, M. (2022). Application of Biomagnetic fluid dynamics modelling for simulation of flow with magnetic particles and variable fluid property over a stretching cylinder. *Mathematics and Computers in Simulation, 199*, 438–462.

[31] Gnaneswara, R., Ahmed, M., and Abbas, W. (2021). Modeling of MHD fluid flow over an unsteady stretching sheet with thermal radiation, variable fluid properties and heat flux. *Math. Comput. Simulat., 185*, 583–593.

[32] Ashraf, M., Abbas, A., Zia, S., Chu, Y., and Khan, I. (2020). Computational analysis of the effect of nanoparticle material motion on mixed convection flow in the presence of heat generation and absorption. *Computers, Materials & Continua, 65*, 1809–1823.

[33] Reddy, Y. D., and Goud, B. S. (2022). Comprehensive analysis of thermal radiation impact on an unsteady MHD nanofluid flow across an infinite vertical flat plate with ramped temperature with heat consumption. *Results in Engineering, 17*, 100796.
[34] Annord Mwapinga. (2012). Computational modeling of arterial blood flow in the presence of body exercise. University of Dar es Salaam.
[35] Harjeet Kumar, Chandel, R. S., Sanjeev Kumar, and Sanjeet Kumar. (2013). A mathematical model for blood flow through a narrow catheterized artery. International Journal of Theoretical & Applied Sciences, 5(2), 101–108.
[36] Voltairas, P. A., Fotiadis, D. I., and Michalis, L. K. (2002). Hydrodynamics of magnetic drug targeting. Journal of Biomechanics, 35(6), 813–821.
[37] Anderson, H. I., and Valnes, O. A. (1998). Flow of a heated ferrofluid over a stretching sheet in the presence of a magnetic dipole. *Acta Mechanica, 128*(1–2), 39–47.
[38] Misra, J. C., Shit, G. C., and Rath, H. J. (2008). Flow and heat transfer of an MHD viscoelastic fluid in a channel with stretching walls: some applications to hemodynamics. *Computers and fluids, 37*, 1–11.
[39] Tzirtzilakis, E. E. (2008). Biomagnetic fluid flow in a channel with stenosis. Physica D: Nonlinear Phenomenna, 237(1), 66–81.
[40] Tzirtzilakis, E. E. (2015). Biomagnetic fluid flow in an aneurysm using ferrohydrodynamics principles. Physics of Fluids, 27, 061902.

Biographies

Rayhan Prodhan got the bachelor's degree in Mathematics from University of Dhaka in 2016 and the Master's degree in Applied Mathematics from University of Dhaka in 2017. Since 2021, he has been working as a Lecturer at the Department of Mathematics, Faculty of Science, Jashore University of Science and Technology, Jashore-7408. His research focuses on

the modeling, analysis and implementation of numerical simulation of fluid flow problems, and analysis their appropriate applications.

Mohammad Ferdows received his Ph.D. degrees from the Department of Mechanical Engineering, Tokyo Metropolitan University, Japan. He worked as a Postdoctoral Research Associate at several Institute/University and also worked as Professor and Visiting Professor in Louisiana Tech University, King Abdulaziz University, King Abdullah University of Science and Technology. Currently he is working as Professor at the Department of Applied Mathematics, University of Dhaka, Bangladesh. His research interests are in fluid mechanics, transport phenomena and biomedical flow phenomena.

J. C. Misra received his D.Sc. in Mathematics from Calcutta University, India. He mainly focuses on Mechanics, Pressure gradient, Flow, Magnetohydrodynamics and Thermodynamics. His Mechanics research incorporates elements of Numerical analysis and Peristalsis. The various areas that he examines in his Peristalsis study include Wave propagation, Non-Newtonian fluid and Transport phenomena. His biological study spans a wide range of topics, including Critical ionization velocity, Porosity and Darcy number.

J. C. Misra interconnects Volumetric flow rate and Shear stress in the investigation of issues within Flow. His Newtonian fluid research incorporates themes from Theoretical physics and Blood flow.

Efstratios Tzirtzilakis is professor at the Department of Mechanical Engineering, University of the Peloponnese, Greece. He has a degree in Mathematics, an MSc in Applied Mathematics, and a PhD in Biomagnetic Fluid Dynamics (BFD). His research field lies in Computational Fluid Mechanics.

M. G. Murtaza received the bachelor's degree in Mathematics from University of Dhaka in 2006, the master's degree in Applied Mathematics from University of Dhaka in 2008, and the philosophy of doctorate degree (Ph.D.) in Applied Mathematics from University of Dhaka in 2020. Since 2020, he has been working as an Associate professor at the Department of Mathematics, Faculty of Science, Comilla University, Cumilla-3506, Bangladesh. His research focuses on the modeling, analysis and implementation of numerical simulation of fluid flow problems with Blood flow, and analysis their appropriate applications.